Electronic structure of an ordered Pb/Ag(111) surface alloy: Theory and experiment

D. Pacilé,[1,2] C. R. Ast,[1,3] M. Papagno,[1,2] C. Da Silva,[1,4] L. Moreschini,[1] M. Falub,[1] Ari P. Seitsonen,[5] and M. Grioni[1]
[1]*Institut de Physique des Nanostructures, Ecole Polytechnique Fédérale de Lausanne, CH-1015 Lausanne, Switzerland*
[2]*Istituto Nazionale di Fisica Nucleare (INFN) and Dipartimento di Fisica, Universitá della Calabria, 87036 Arcavacata di Rende, Cosenza, Italy*
[3]*Max-Planck-Institut für Festkörperforschung, 70569 Stuttgart, Germany*
[4]*Laboratoire de Cristallographie, CNRS, Boîte Postale 166, 38042 Grenoble Cedex 09, France*
[5]*Physikalisch Chemisches Institut der Universität Zürich, Winterthurerstrasse 190, CH-8057 Zürich and CNRS et IMPMC, Université Pierre et Marie Curie, 4 place Jussieu, case 115, F-75252 Paris, France*

(Received 25 January 2006; revised manuscript received 28 April 2006; published 23 June 2006)

We have studied by angle-resolved photoelectron spectroscopy (ARPES) the band structure of the ordered surface alloy obtained by the deposition of 0.33 monolayers of Pb on the Ag(111) surface. We observe several dispersing features which are well described as Pb-Ag hybrid bands by a band structure calculation performed within the generalized gradient approximation of density functional theory. We also find that a band of mixed Pb p_z and Ag s character is split in momentum space. We interpret this splitting as the combined result of spin-orbit interaction and broken inversion symmetry at the surface.

DOI: 10.1103/PhysRevB.73.245429 PACS number(s): 73.20.At, 71.70.Ej, 79.60.Dp, 71.15.Mb

I. INTRODUCTION

Surface alloying is a subject of fundamental interest with applications in diverse fields such as catalysis, corrosion, and surface hardening. Since surface-specific species may form between pairs of metals that are not miscible in the bulk, surface alloying offers a real possibility of designing, e.g., novel catalysts at the nanoscale, with improved chemical properties, in terms of overall activity and improved selectivity.[1] The formation of surface alloys has been observed in numerous systems,[2–8] and much work has been especially devoted to the study of their structural properties. Since the adatoms selectively replace substrate atoms of the topmost monolayer, large hybridization effects are expected to yield new two-dimensional electronic structures, which are at the origin of the enhanced physical properties. Modern angle-resolved photoemission spectroscopy (ARPES) with high energy and momentum resolution is ideally suited to characterize these electronic states.

We address here the electronic structure of the $(\sqrt{3}\times\sqrt{3})R30°$ Pb/Ag(111) surface alloy, which is obtained by depositing one-third of a monolayer (ML) of Pb on the clean Ag(111) surface. The structural properties of this ordered surface alloy have been previously studied by low-energy electron diffraction, reflection high-energy electron diffraction, and transmission electron microscopy.[9,10] Recently, scanning tunneling microscopy and synchrotron radiation surface x-ray diffraction studies[11,12] showed that Pb atoms are embedded in the Ag topmost layer [Fig. 1(a)] where they replace every third Ag atom, producing a long-range-ordered structure. A mixed phase is then formed in spite of the large mismatch between the Pb and Ag atomic radii (Pb is 17% larger) and of a strong tendency toward phase separation in the bulk.

We report ARPES data that illustrate the extensive hybridization between the Pb- and substrate-derived electronic states, and the formation of a new surface electronic structure. The experimental band structure is well described by a slab superlattice calculation performed within the generalized gradient approximation (GGA) of density functional theory (DFT). However, we also observe that a band of mixed Pb p_z and Ag s character is split in momentum space and, as a consequence, in energy. This splitting is not reproduced by the calculated bands. We attribute it to the joint effect of inversion symmetry breaking at the surface, and of spin-orbit interaction, which is not included in the calculation.

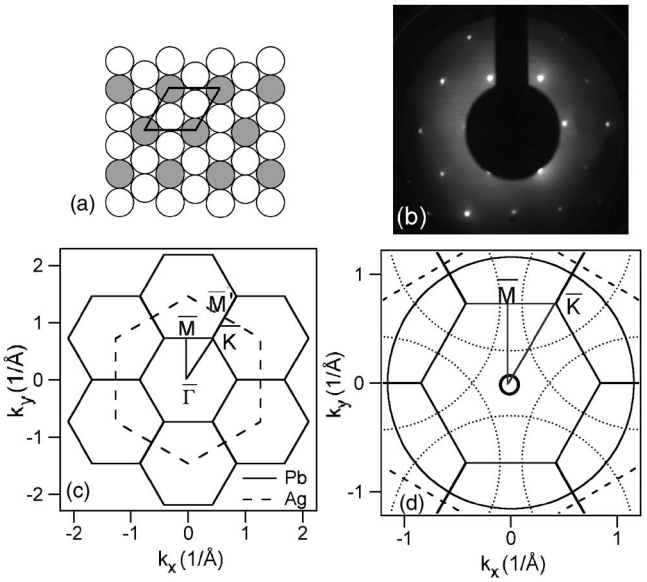

FIG. 1. The $(\sqrt{3}\times\sqrt{3})R30°$ Pb/Ag(111) ordered alloy. (a) Real space structure, showing lead atoms (gray) in substitutional sites. The hexagonal primitive cell is also shown. (b) The corresponding LEED image. (c) The substrate (dashed) and superlattice (solid line) hexagonal surface Brillouin zones. (d) Schematic Fermi surface contours of the Ag surface state (small inner circle) and bulk valence band (large circle). The dotted circles are centered on the adjacent Brillouin zones and represent umklapps of the main Fermi surface.

II. EXPERIMENT

Photoemission data were collected by a Scienta ESCA-300 spectrometer equipped with a high-brilliance monochromatized He lamp. The mapping of the electronic states along a given azimuth was performed by rotating the sample manipulator to vary the polar emission angle of the outgoing photoelectrons. Parallel detection in the angular mode of the analyzer allowed the simultaneous collection of ARPES spectra within an angular window of $\sim 10°$ in the perpendicular direction in k space. The angular resolution was better than $\pm 0.5°$, and the total energy resolution was $\Delta E = 10$ meV, as determined at the Fermi edge of a polycrystalline Ag film.

Clean Ag(111) surfaces were prepared by cycles of Ar^+ sputtering (at 500 eV) followed by an annealing at 800 K by backside electron bombardment. Sputter-annealing cycles were repeated until a clean and well-ordered surface was obtained, as judged by x-ray photoelectron spectroscopy and low-energy electron diffraction (LEED). The quality of the clean surface was also checked by ARPES, namely, by inspection of the L-gap Shockley-type surface state.[13–15] Lead was evaporated from a molybdenum crucible, at a deposition rate of about 1.0 Å/min, with the Ag substrate kept at room temperature. The $(\sqrt{3}\times\sqrt{3})R30°$ Pb/Ag(111) superstructure was observed after Pb depositions in the range of 0.5–1.0 Å, with one Pb ML corresponding to 2.6 Å. The best surfaces [Fig. 1(b)] in terms of sharpness of the LEED spots and of the ARPES line shapes were obtained for Pb depositions slightly above the nominal coverage of 0.33 ML, followed by an annealing at 600 K to remove the extra lead atoms and to reorder the structure.

III. CALCULATIONAL METHODS

The DFT calculations were performed employing both the local density approximation (LDA) and the generalized gradient approximation as the exchange-correlation functional in the Kohn-Sham equations.[16] A slab in a supercell geometry consisting of 22 layers was regarded as necessary in order to decouple the surface states of the clean Ag(111) surface. Every third Ag atom was substituted by a Pb atom at one surface of the slab. All the atomic coordinates, with the only exception of the z coordinates of the two middle layers, were allowed to relax. We used the Kohn-Sham eigenvalues as an estimate of the band structure of the surfaces; the two approximations, LDA and GGA, yield qualitatively the same results, but the position of the surface states is slightly different. Here we shall only discuss results obtained with the GGA of Perdew *et al.*[17] We employed a plane wave basis set up to the cutoff energy of 60 Ry and norm-conserving pseudopotentials generated according to the scheme of Troullier and Martins.[18] For Pb we included the $5d$ states in the valence of the pseudopotential and created a pseudopotential with $r_c = 2.0$ bohr as the core radius for all the l channels. We used ten k points[19] in the irreducible wedge of the surface Brillouin zone of the $(\sqrt{3}\times\sqrt{3})R30°$ fcc(111) structure, and nearly 20 Å of vacuum to separate the two sides of the slab well.

IV. RESULTS AND DISCUSSION

A. ARPES measurements

Figure 1(a) illustrates the $(\sqrt{3}\times\sqrt{3})R30°$ Pb/Ag(111) structure, where Pb atoms occupy substitutional sites. The corresponding LEED pattern and reciprocal space structure are shown in Figs. 1(b) and 1(c). The first surface Brillouin zone of the substrate and superlattice are rotated by 30° with respect to each other. In the following we will always refer to the high-symmetry directions of the superlattice, as in Fig. 1(c).

Figure 2 illustrates a typical set of energy distribution curves for the $\sqrt{3}\times\sqrt{3}$ alloy, obtained along the $\bar{\Gamma}\bar{K}$ and $\bar{\Gamma}\bar{M}$ high-symmetry directions. It shows a prominent band with a negative effective mass, and some weaker features crossing the Fermi level (E_F) on both sides of $\bar{\Gamma}$. The dispersive branches marked by gray symbols and crossing E_F at the same angular distance from the zone center belong to the sp-derived Ag bulk valence band. Additional dispersive structures are visible besides these branches. They have no counterpart in the electronic structure of the clean Ag(111) substrate, and therefore belong to the alloy structure. The overall alloy band structure is illustrated by an ARPES intensity map [Fig. 3(a)] extracted from the data of Fig. 2. It shows the binding energy vs parallel wave vector on a gray scale, with black corresponding to the highest photoemission intensity. A high-resolution closeup of the band structure around the $\bar{\Gamma}$ point is illustrated by Fig. 3(b). The experimental band dispersion for the whole angular range of Fig. 2 is summarized in Fig. 3(c). Solid lines correspond to Ag bands and dotted ones to new bands of the alloy. The Ag surface state, which is visible around the $\bar{\Gamma}$ point on the clean (111) surface, is removed by the interaction with the Pb-derived states. The Ag sp valence-band dispersion is marked by thick lines, while thin lines correspond to surface umklapps, as can be deduced from Fig. 1(d). As to the alloy bands, the experimental dispersion hints at a nearly parabolic band with a maximum just above E_F at $\bar{\Gamma}$. Weak sidebands, offset in parallel momentum, follow the dispersion of the main band. A second band exhibits a minimum at ~ 3.5 eV at the $\bar{K}$ point, and a saddle point at the $\bar{M}$ point, with a maximum along the $\bar{\Gamma}\bar{K}\bar{M}'$ direction, and a minimum along $\bar{\Gamma}\bar{M}\bar{\Gamma}'$.

B. Calculated band structure

Shown in Fig. 4 are the projections of the orbitals in the Pb/Ag(111) system onto the atomic orbitals around the Pb [Fig. 4(a)] and Ag [Fig. 4(b)] atoms. The size of the symbols is proportional to the overlap of the band in question with the radial atomic orbital times the spherical harmonic Y_{lm}. The band gap in the projected bulk band structure is shown with a continuous line around $\bar{\Gamma}$. We see that the state slightly above the Fermi energy at and around $\bar{\Gamma}$ has mainly sp_z character at the Pb site. The band with a maximum at ~ 1.8 eV at $\bar{\Gamma}$, dispersing downward along the $\bar{\Gamma}\bar{M}$ and $\bar{\Gamma}\bar{K}$ lines, has almost purely p_{xy} character. Along $\bar{\Gamma}\bar{K}$ it splits into an initially downward-dispersing $p_{x,y}$ band, which then

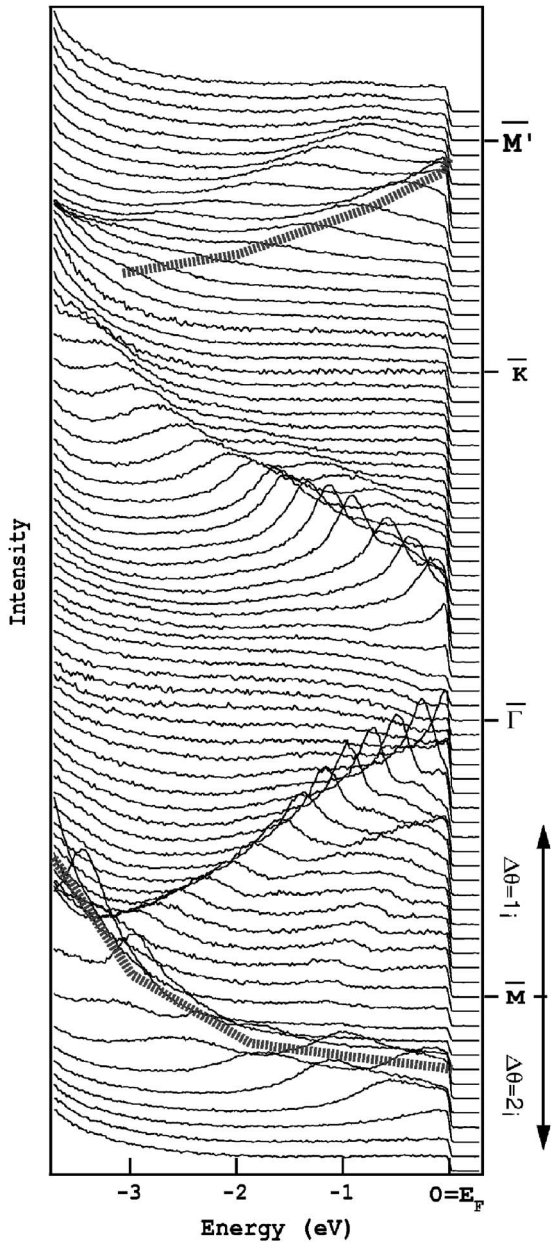

FIG. 2. Energy distribution curves obtained along the $\overline{\Gamma KM'}$ (upper part) and $\overline{\Gamma M\Gamma'}$ (lower part) high-symmetry directions. Each curve corresponds to a different polar emission angle. The angular step is 1° above the $\bar{M}$ point and 2° below. Gray dotted lines underline the dispersion of the *sp*-derived Ag bulk valence band.

changes to sp_z-type character and starts dispersing upward. We note that the two new strong surface states have also weight at the surface Ag atoms [Fig. 4(b)]. At $\bar{\Gamma}$ the lower band has mainly Ag *s* and the upper band Ag d_{xy,x^2-y^2} character.

C. Discussion

The overall agreement between the experimental results [Figs. 3(c)] and the calculated band structure (Fig. 4) is quite satisfactory. Theory confirms the hybrid nature of the bands of the alloy [dotted lines in Fig. 3(c)], and accurately describes their dispersion, including the location of their extrema, and the size of the corresponding Fermi surface. Nevertheless, the calculation does not reproduce all the sidebands of the main band centered at $\bar{\Gamma}$. In fact, it predicts two closely separated bands along $\overline{\Gamma K}$, whereas the two bands are widedly spaced along $\overline{\Gamma M}$. Unexpected weak sidebands of the innermost parabolic band are clearly visible in both high-symmetry directions in the high-resolution data of Fig. 3(b). A more detailed analysis of the experimental data clarifies the nature of the weak features observed by ARPES. Figure 5(a) shows a momentum distribution curve (MDC), i.e., a constant-energy cut through the ARPES intensity map of Fig. 3(a), taken just below E_F [E=0.14 eV; dashed line in Fig. 3(a)]. The MDC shows several peaks in both the $\overline{\Gamma K}$ and $\overline{\Gamma M}$ directions, with each peak representing a dispersing ARPES feature in Fig. 3. Peaks A and A', which belong to the main band, exhibit shoulders (B and B') in correspondence with the sidebands. This can be further visualized by the two-dimensional constant-energy contours of Fig. 5(b). They illustrate the k-space distribution of the ARPES intensity at E=0.14 eV, within two stripes $\sim$0.3 Å^{-1} wide and centered respectively along the $\overline{\Gamma K}$ and $\overline{\Gamma M}$ directions. Instead of the single circular profile expected for an isotropic parabolic band, we observe two concentric circles, of unequal intensity, centered at $\bar{\Gamma}$. At larger wave vectors, in correspondence to peaks C and C' of Fig. 5(a), the intensity plot also exhibits circular arcs of larger radii, which can be attributed to umklapps of the bulk Ag *sp* band [Fig. 1(d)].

The observation of two circular concentric constant-energy lines bears strong analogies with similar results for the clean Au(111) surface.[14,20] It is now established that the dispersion of the Au(111) surface state is modified by the spin-orbit interaction which splits, in momentum space, states of opposite spin. This effect, known as the Rashba-Bychkov effect in semiconductors,[21] was originally predicted for a two-dimensional electron gas at a semiconductor heterojunction. The surface breaks the inversion symmetry of the bulk crystal, opening up the possibility for the spin degeneracy to be lifted in the presence of spin-orbit coupling. The energy splitting is $\Delta E=2\alpha_R k_\parallel$ and, in the free-electron limit, the Rashba parameter α_R is simply proportional to the gradient of the surface potential. The resulting band $E(k_x,k_y)$ can be visualized as the surface obtained by rotating around the surface normal two parabolas offset by a quantity $\Delta k_\parallel = (m^*/\hbar^2)\alpha_R$ on opposite sides of $\bar{\Gamma}$. The model also predicts a peculiar spin arrangements in the split bands, with spins rotating within the surface plane along the concentric constant-energy contours, and a characteristic asymmetry in the distribution of the photoelectron intensity reflecting the parity of the surface states.[22] Both features have been experimentally verified for Au(111), but the size ($\sim$110 meV) of the measured energy splitting of the two branches greatly exceeds the predictions of the simple free-electron model. More recently, it has been shown by a tight-binding approach that the splitting is controlled not only by the gradient of the surface potential, but also by the magnitude of the atomic spin-orbit interaction.[23] The influence of atomic parameters was confirmed by ARPES experiments on chemically disor-

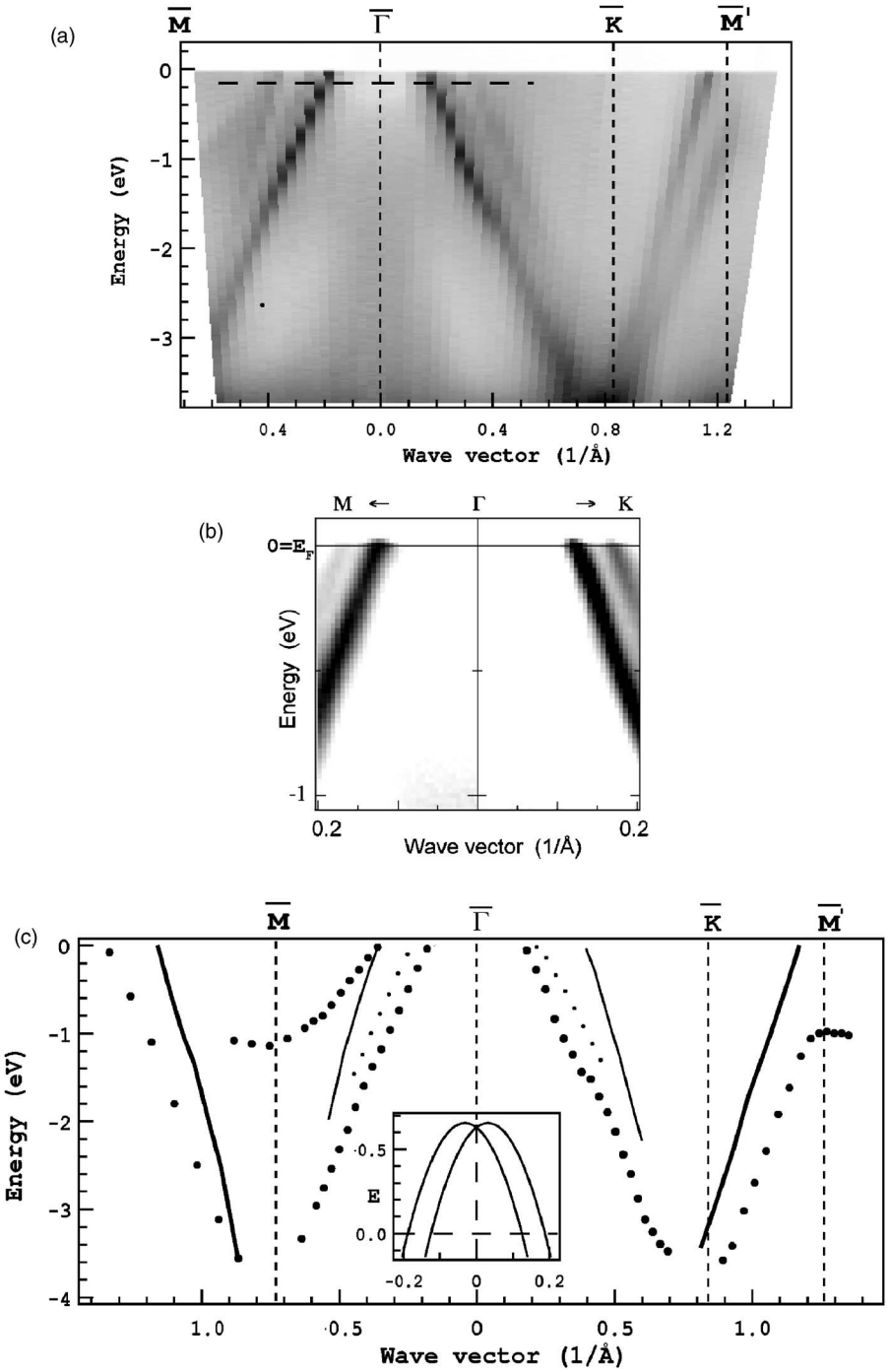

FIG. 3. (a) ARPES intensity plot extracted from Fig. 2. (b) High-resolution ARPES image of the band structure near the $\bar{\Gamma}$ point, illustrating the momentum splitting of a parabolic surface band. (c) Schematic dispersion of all the dispersive features for the full angular range of Fig. 2. Thick solid line, Ag *sp* bulk band; thin solid line, surface umklapp bands from the Ag bulk band; solid symbols, hybrid Pb-Ag bands. In the inset the fit of the experimental data extended above the Fermi level is shown.

dered Au-Ag alloys grown at the Au(111) surface, where the spin-orbit splitting of the two subbands could be tuned as a function of the alloy composition.[24] It is also supported by the large splitting observed at the (111) surface of the high-Z element bismuth.[25]

The Rashba scenario provides a natural explanation for the ARPES results of the Pb-Ag(111) surface alloy. We fitted the measured dispersion [Fig. 3(b)] by two identical parabolic bands offset by an amount $\pm\Delta k_{\|}$ away from the $\bar{\Gamma}$ point, as shown in the inset of Fig. 3(c). The observed unequal distribution of spectral weight among the various branches is consistent with the model of Ref. 22, when the collection geometry and the degree of linear polarization of our photon beam are taken into account. The energy maximum of the two parabolas was set to 0.66 eV above the Fermi level, as determined by an independent scanning tunneling spectroscopy measurement,[11] whereas the other coefficients of the parabola were determined by the best fit to the data. This procedure yields $\Delta k_{\|}=0.03$ Å^{-1}, an effective mass $m^*=-0.15m_e$, and a Rashba parameter $\alpha_R=1.42$ eV Å^{-1}.

This interpretation of the data in terms of spin-split bands is strongly supported by our recent ARPES results on the closely related Bi/Ag(111) $\sqrt{3}\times\sqrt{3}$ surface alloy.[26] Bismuth is the element immediately following Pb in the periodic table, and the Bi-Ag and Pb-Ag alloys exhibit strong structural and electronic similarities. As a result, the split band

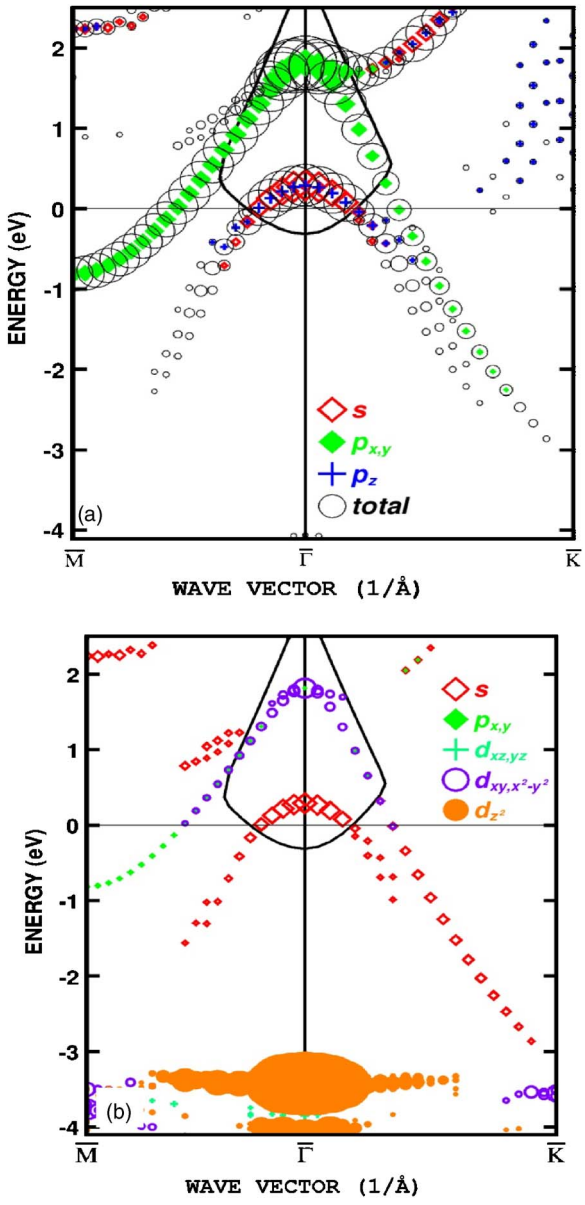

FIG. 4. (Color online) (a) Projection of the orbitals of the Pb/Ag(111) alloy onto the atomic orbitals around the Pb atoms. The size of the symbols represents the magnitude of the overlap. The different symbols denote s, empty diamonds, $p_{x,y}$, filled diamonds, p_z, crosses, and the sum over projections on all s, p and d orbitals, empty circles. (b) Projection onto the atomic orbitals around the Ag surface atoms: s, empty diamonds, $p_{x,y}$, filled diamonds, $d_{xz,yz}$, crosses, d_{xy,x^2-y^2}, empty spheres, and d_{z^2}, filled spheres. Projections are not shown for components with a negligible overlap.

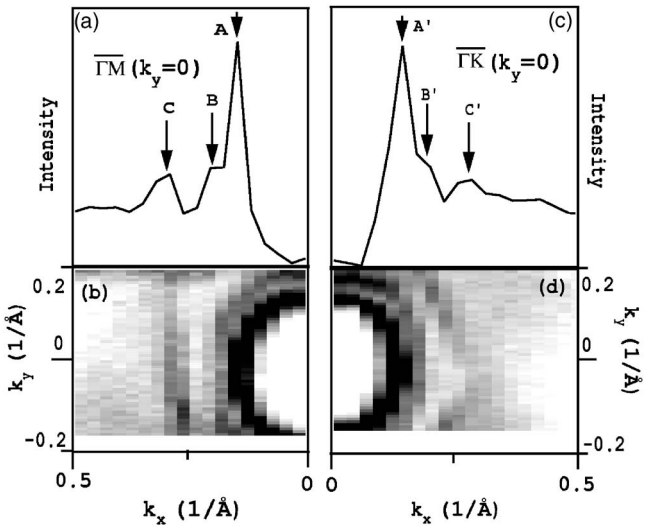

FIG. 5. (a),(c) MDCs measured at $E=0.14$ eV [dashed line in Fig. 3(a)] along the $\overline{\Gamma M}$ direction and the $\overline{\Gamma K}$ one, respectively. (b),(d) Corresponding ARPES constant-energy ($E=0.14$ eV) intensity profile. The double circumference centered at $\bar{\Gamma}$ illustrates the splitting of the corresponding hybrid band. The k_x axis is along (a),(b) $\overline{\Gamma M}$ and (c),(d) $\overline{\Gamma K}$.

around $\bar{\Gamma}$, which is only partially occupied for Pb-Ag, is completely filled by the additional electron in Bi, according to a simple rigid-band scheme. The band structure, which becomes fully accessible to ARPES, is in excellent agreement with the spin-split scenario sketched in the inset of Fig. 3(c). A similar analysis of the Bi-Ag data yields $\Delta k_{\parallel} = 0.16$ Å^{-1}. The larger value is, at least in part, a consequence of the $6p$ atomic spin-orbit splitting, which is larger in Bi (2.16 eV) than in Pb (1.75 eV).[27]

V. SUMMARY

We have investigated the electronic structure of the $(\sqrt{3} \times \sqrt{3})R30°$ Pb/Ag(111) alloy obtained by a surface reaction of 1/3 of a ML of Pb deposited on a clean Ag(111) substrate. Our ARPES results show that the formation of the ordered surface alloy is accompanied by a strong modification of the surface electronic structure of the substrate. The topology and dispersion of the new surface bands of mixed Pb-Ag character are accurately described by a DFT slab calculation. One of these bands is split in momentum space by the spin-orbit interaction, in close analogy with the clean Au(111) surface, and especially with the related Bi/Ag(111) surface alloy. These results illustrate the connection between surface alloying, atomic structure, and spin-orbit splitting. They show that large spin splittings may be achieved as a result of surface alloying between a high-Z overlayer and a metallic substrate. They also indicate an interesting alternative route to that already explored which consists in modifying the surface potential by the absorption of adatoms.[28]

ACKNOWLEDGMENTS

We gratefully acknowledge insightful remarks by G. Wittich, P. Wahl, K. Kern, and J. Sorel. This work was supported by the Swiss National Science Foundation. The DFT calculations have been performed at Rechenzentrum Garching der Max-Planck-Gesellschaft.

[1] M. Chen, D. Kumar, C. Yi, and D. W. Goodman, Science **310**, 291 (2005).
[2] H. Roder, R. Schuster, H. Brune, and K. Kern, Phys. Rev. Lett. **71**, 2086 (1993).
[3] S. Oppo, V. Fiorentini, and M. Scheffler, Phys. Rev. Lett. **71**, 2437 (1993).
[4] U. Bardi, Rep. Prog. Phys. **57**, 939 (1994).
[5] J. Tersoff, Phys. Rev. Lett. **74**, 434 (1995).
[6] J. L. Stevens and R. Q. Hwang, Phys. Rev. Lett. **74**, 2078 (1995).
[7] P. D. Quinn, C. Bittencourt, and D. P. Woodruff, Phys. Rev. B **65**, 233404 (2002).
[8] X. K. Shu, P. Jiang, and J. G. Che, Surf. Sci. **545**, 199 (2003).
[9] K. J. Rawlings, M. J. Gibson, and P. J. Dobson, J. Phys. D **11**, 205 (1978).
[10] K. Takayanagi, D. M. Kolb, K. Kambe, and G. Lehmpfuhl, Surf. Sci. **104**, 527 (1981); **100**, 407 (1980).
[11] G. Wittich *et al.* (private communication).
[12] J. Dalmas, H. Oughaddou, C. Leandri, J-M. Gay, G. Le Glay, G. Treglia, B. Aufray, O. Bunk, and R. L. Johnson, Phys. Rev. B **72**, 155424 (2005).
[13] R. Paniago, R. Matzdorf, G. Meister, and A. Goldmann, Surf. Sci. **336**, 113 (1995).
[14] F. Reinert, G. Nicolay, S. Schmidt, D. Ehm, and S. Hüfner, Phys. Rev. B **63**, 115415 (2001).
[15] G. Nicolay, F. Reinert, S. Schmidt, D. Ehm, P. Steiner, and S. Hüfner, Phys. Rev. B **62**, 1631 (2000).
[16] P. Hohenberg and W. Kohn, Phys. Rev. **136**, B864 (1964); W. Kohn and L. J. Sham, Phys. Rev. **140**, A1133 (1965).
[17] J. P. Perdew, J. A. Chevary, S. H. Vosko, K. A. Jackson, M. R. Pederson, D. J. Singh, and C. Fiolhais, Phys. Rev. B **46**, 6671 (1992).
[18] N. Troullier and J. L. Martins, Phys. Rev. B **43**, 1993 (1991).
[19] S. L. Cunningham, Phys. Rev. B **10**, 4988 (1974); Ari P Seitsonen, Ph.D. thesis, Technische Universität Berlin, 2000, http://edocs.tu-berlin.de/diss/2000/seitsonen_ari.htm
[20] S. LaShell, B. A. McDougall, and E. Jensen, Phys. Rev. Lett. **77**, 3419 (1996).
[21] Y. A. Bychkov and E. I. Rashba, JETP Lett. **39**, 78 (1984).
[22] J. Henk, M. Hoesch, J. Osterwalder, A. Ernst, and P. Bruno, J. Phys.: Condens. Matter **16**, 7581 (2004).
[23] L. Petersen and P. Hedegård, Surf. Sci. **459**, 49 (2000).
[24] H. Cercellier, Y. Fagot-Revurat, B. Kierren, F. Reinert, D. Popovic, and D. Malterre, Phys. Rev. B **70**, 193412 (2004).
[25] Y. M. Koroteev, G. Bihlmayer, J. E. Gayone, E. V. Chulkov, S. Blugel, P. M. Echenique, and Ph. Hofmann, Phys. Rev. Lett. **93**, 046403 (2004).
[26] Ch. R. Ast *et al.*, cond-mat/0509509 (unpublished).
[27] L. Ley, S. P. Kowalczyk, F. R. McFeely, and D. A. Shirley, Phys. Rev. B **10**, 4881 (1974).
[28] E. Rotenberg, J. W. Chung, and S. D. Kevan, Phys. Rev. Lett. **82**, 4066 (1999).